

## DIGITAL MICROSCOPY AND IMAGE ANALYSIS APPLIED TO COMPOSITE MATERIALS CHARACTERIZATION <sup>(1)</sup>

*Sidnei Paciornik* <sup>(2)</sup>  
*José Roberto M. d'Almeida* <sup>(3)</sup>

### **Abstract**

Digital Microscopy was employed to characterize the microstructure of fiber-reinforced composite tubes manufactured by filament winding. Optical Microscopy was used for void characterization while Scanning Electron Microscopy was used for fiber and layer analysis. Acquired images were assembled in mosaics to reveal the microstructure of different cross-sections of the sample. Image processing was employed to detect either voids or individual fibers and measure their size, shape and spatial distribution. Void spatial distribution was analyzed with two different methods – local analysis and the tessellation method – revealing different behaviors along different cross-sections. Fiber layers were automatically detected and their average winding angle and dispersion were analyzed.

**Key-words:** composites, filament winding, voids, image analysis, digital microscopy

---

<sup>1</sup> ABM-TMS International Conference, July 26-30, 2010, Rio de Janeiro, Brazil

<sup>2</sup> D. Sc., Associate Professor – DEMa PUC-Rio

<sup>3</sup> D. Sc., Associate Professor – DEMa PUC-Rio

## 1. INTRODUCTION

The microstructural characterization of a material is a key step to understand its practical engineering properties. For composites, the microstructural characterization is even more critical, because of the many possible arrangements between the reinforcing phase and the matrix. When one wants to characterize a composite, the volume or mass fraction of the phases is the most commonly described parameter. This is a direct consequence of the strong influence that the volume fraction of the reinforcing phase has on the properties of the composite.

However, for heterogeneous materials like fiber-reinforced composites, the influence of the microstructure on the engineering properties is critical, and besides the volume fraction, the complete understanding of composites properties requires the determination of several microstructural parameters such as size, orientation and spatial distribution of the fibers and of possible defects. In fact, voids are a common feature appearing during the usual manufacturing processes [1,2,3], and even for aeronautical grade resin matrix composites, the presence of voids is allowed although restricted to low percentages. But, voids are stress concentrators and can act as crack initiation points [4]. Therefore, besides their volume fraction, other microstructural characteristics such as their spatial distribution and aspect ratio should be carefully evaluated [1].

Although measuring the volume fraction of voids or particles is a common practice [5,6], the spatial distribution of these microstructural parameters can also be of relevance [1]. By characterizing the preferred distribution of voids, one can access information about the manufacturing process itself. For example, for filament winding parts, voids preferentially distributed among the tows of fibers are probably due to an inappropriate level of stress when the fibers are being wound around the mandrel [7]. On the other hand, voids on resin rich areas can originate from entrapped air bubbles generated during the stirring of the resin or are due to the evolution of by-products during the cure of the resin. Moreover, it can be of interest to determine if the voids are clustered or uniformly distributed on the cross section of the composite.

The use of filament winding also brings a new level of complexity to the characterization of the reinforcement phase, as the composite is made up of a series of layers, with different thickness and fiber orientations. So it is important to discriminate individual fibers, their orientations, and groups of similarly oriented fibers forming layers. Gathering all this information is, however, not easy using the traditional methods of microstructural analysis.

Digital Microscopy (DM) is the convergence of microscope automation, digital image acquisition, processing and analysis. The use of DM allows a complete characterization of a sample in fully automated procedures. Online acquired images can be automatically treated and the desired features can be discriminated and analyzed. Moreover, a large number of fields, comprising thousands of objects can be quickly analyzed, providing high statistical accuracy [8].

In this work, the microstructure of a glass fiber-reinforced composite pipe fabricated by filament winding was fully characterized by Digital Microscopy. Both Optical Microscopy (OM) and Scanning Electron Microscopy (SEM) were employed, respectively, for void and fiber characterization.

## 2. EXPERIMENTAL

### 2.1 Specimen selection and preparation

Polyester matrix–filament wound glass fiber pipes used for the transport of water in offshore oil production facilities and having a nominal internal diameter of 200 mm and 7 mm thickness, were analyzed in this work. The pipes were sectioned in rings 25 mm thick that were then cut into 4 quadrants. Axial and circumferential samples were prepared for microstructural analysis (Figure 1). The preparation followed the usual procedures of grinding and polishing, from silicon carbide grit (#100) to alumina powder (0.5  $\mu\text{m}$ ). Whenever possible the cutting operation was performed using a low speed saw, to avoid excessive damage of the glass fibers [9].

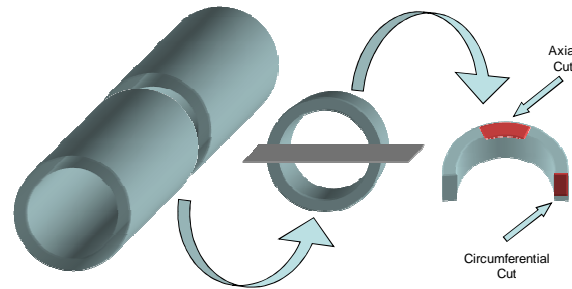


Figure 1 - Illustration of axial and circumferential samples obtained from the composite tube.

### 2.2 Image Acquisition

To characterize the microstructure in respect to the distribution of voids and fibers, as well as their spatial orientation, it was desirable to obtain images combining high magnification and a large area of analysis. These requisites are not fulfilled by a single image. Therefore, it was necessary to capture several images, with the same magnification, and to join them together generating a mosaic image [10].

For void characterization, the samples were observed by optical microscopy using a Zeiss AxioPlan 2 motorized optical microscope. The use of this computer-controlled equipment, with a motorized x-y-z sample holder, allows controlled sample displacement and the acquisition of a sequence of images with any spatial distribution and with automated focus control [8]. The images were captured using an AxioCam HR digital camera, with 1300 x 1300 pixels resolution.

Image mosaics were constructed by joining low magnification images, obtained using a 5x objective lens (Zeiss EPIPLAN, NA = 0.13). These images covered an entire cross-section of the samples, from the outer to the inner diameter. Each field occupied an area of 2750 x 2180  $\mu\text{m}^2$ , with a spatial resolution of 2.10  $\mu\text{m}/\text{pixel}$ . To cover the entire sample area, 7 fields on the x direction and 3 on the y direction were necessary, leading to a total area of 19.2 x 6.5  $\text{mm}^2$ . This procedure permitted a complete visualization of each sample, clearly revealing the spatial distribution of voids, and allowing the measurement of features on the entire sample.

For fiber and layer characterization the images the samples were observed by scanning electron microscopy, using the backscattered (BSE) mode of image formation. BSE was preferred instead of secondary electrons imaging, because the intensity of the BSE signal is a function of the atomic weight of the elements on the sample. Therefore, a good contrast is obtained between the polymeric matrix and glass fibers. Moreover, the images do not show topographical information, which is beneficial in the image processing steps, as residual artifacts from sample preparation are blurred. The images were captured with 512 x 480 pixels resolution, at a magnification of 200x, corresponding to 0.88  $\mu\text{m}/\text{pixel}$ .

In this case, mosaic images were generated combining 28 images – 4 fields in the x direction and 7 in the y direction. This procedure allowed for a complete visualization of the cross-section, clearly revealing the spatial distribution of the fiber layers, and allowing the measurement of features on the entire sample.

### 3. RESULTS AND DISCUSSION

#### 3.1 Spatial Distribution of Voids

Figure 2a shows the image of a mosaic from a circumferential sample. The larger white rectangle depicted represents one of the 21 (7 x 3) mosaic tiles, also shown magnified in Figure 2b. As one can see, the mosaic offers a global view of the sample, clearly showing the spatial distribution of voids and fibers. In this view, the fibers are mainly aligned perpendicular to the plane of cut and appear as circles. Most large visible voids are also approximately round, as can be seen in Figure 2b. It is worth mentioning that the circumferential sample actually shows the spatial distribution of voids along the axis of the tube.

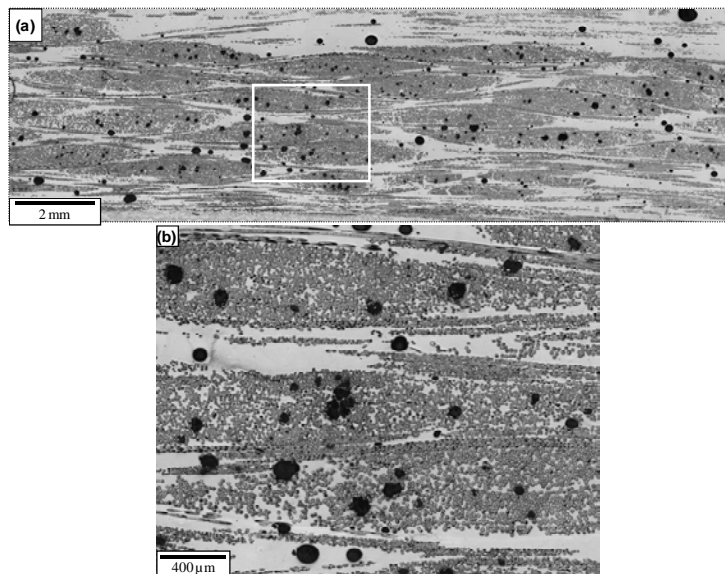


Figure 2 – Circumferential sample. (a) Mosaic image obtained with a 5X objective lens (2.1  $\mu\text{m}/\text{pixel}$ ). (b) Digital magnification of the area outlined by the white rectangle.

Figure 3a shows a mosaic image of an axial cut through the sample. The fibers appear as elongated objects while both round and elongated voids are visible. The presence of very elongated voids (Figure 3b), illustrates the relevance of observing the sample in different orientations. Moreover, such long objects also highlight the usefulness of the mosaic image – in a regular field scan microscopy procedure these objects can be too large to fit any individual field, precluding their accurate characterization of size and shape. Again, it is worth mentioning that the axial sample actually shows the spatial distribution of voids along the circumference of the tube.

Voids can be discriminated by their grey shade. As seen in Figures 2 and 3, they appear darker than the fibers and the polymer matrix. However, small regions of fibers damaged during sample preparation exhibit similar contrast, and may lead to wrong results. Therefore, an image processing and analysis routine was developed to discriminate the several kinds of dark regions appearing on the images, and recognize the voids. This routine is described in detail elsewhere [10]. The results are shown in Figure 4 for a representative field in Figure 2a.

Once voids are reliably recognized, their spatial distribution can be measured. This analysis was performed on the mosaic images, with two different methods: local



mapping and neighborhood analysis. In local mapping the mosaic images were scanned with an analysis window of 250 x 250 pixels and, for each window, two parameters were obtained: void count and void area fraction. To avoid multiple counting of objects at the edges of the windows, a guard frame was used in which voids touching the bottom or left edges of the window were not considered. Thus, if a void straddles an edge between windows it will be counted only once. These parameters were then plotted as contour maps as shown in Figures 5 and 6 for the circumferential and axial samples, corresponding to Figures 2a and Figure 3a.

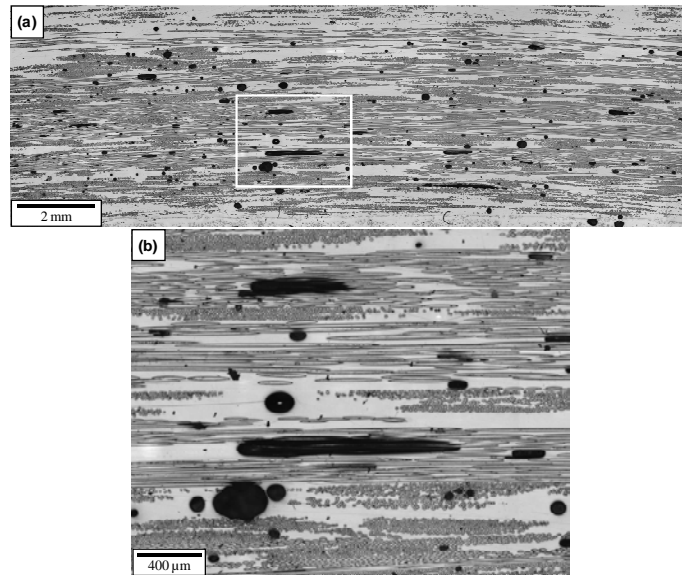


Figure 3 – Axial sample. (a) Mosaic image obtained with a 5X objective lens (2.1  $\mu\text{m}/\text{pixel}$ ). (b) Digital magnification of the area outlined by the white rectangle.

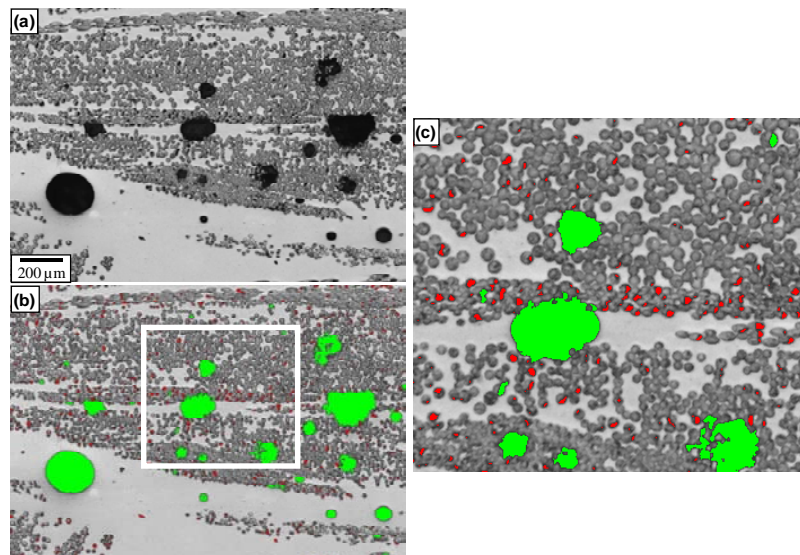


Figure 4 – Void discrimination. (a) Original image (5X objective lens, 2.1  $\mu\text{m}/\text{pixel}$ ). (b) Detected dark objects (green and red). (c) Magnified view of the region outlined in (b) – voids are shown in green while red objects are smaller than 40 pixels in area and correspond to broken fiber tips.

The maps provide a global view of the desired parameters across the whole cross-section, and indicate variations in spatial distribution. Comparing Figure 5 to Figure 6 one can state that the spatial distribution of voids for the circumferential sample is more uniform than for the axial sample. However, even though the maps contain quantitative information, the level of uniformity of the spatial distribution is still deduced in a qualitative way. To obtain a quantitative parameter that describes the uniformity of spatial distribution, a neighborhood analysis was applied.

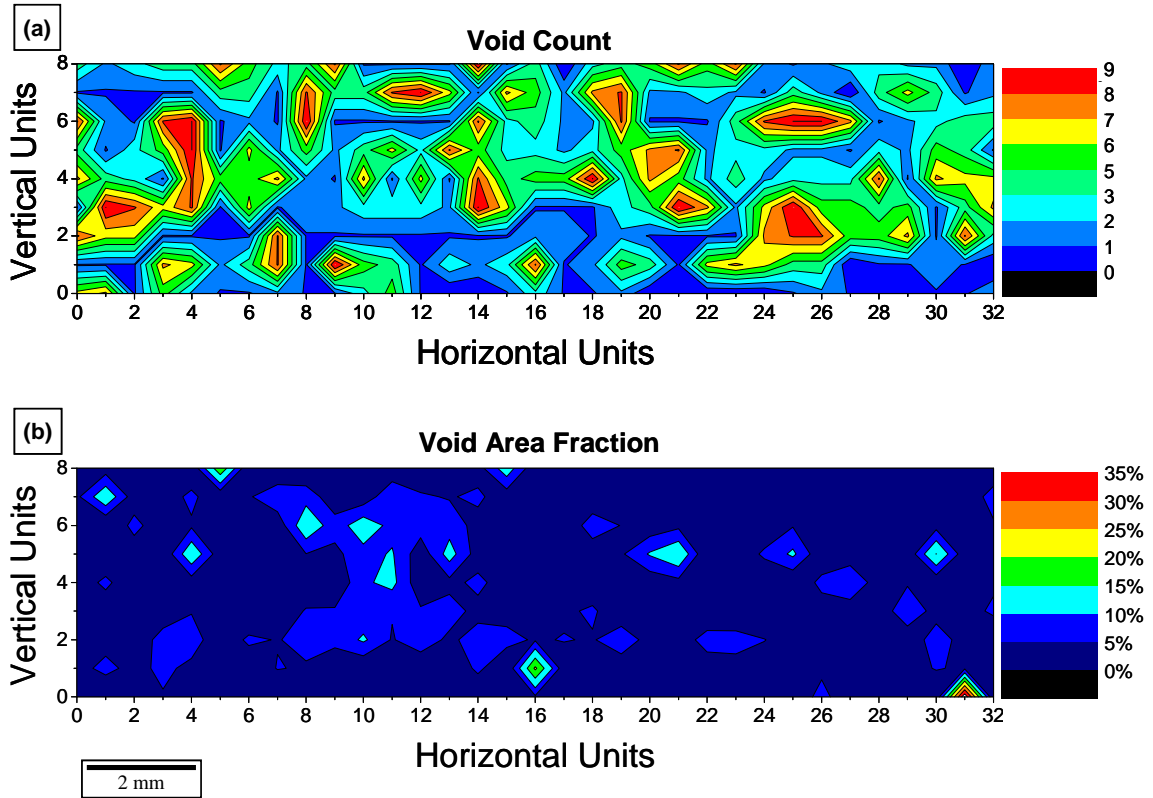


Figure 5 – Local mapping for circumferential sample. (a) Void count. (b) Void area fraction. Horizontal and vertical units refer to the count of 250x250 pixels windows in each direction. See text for details.

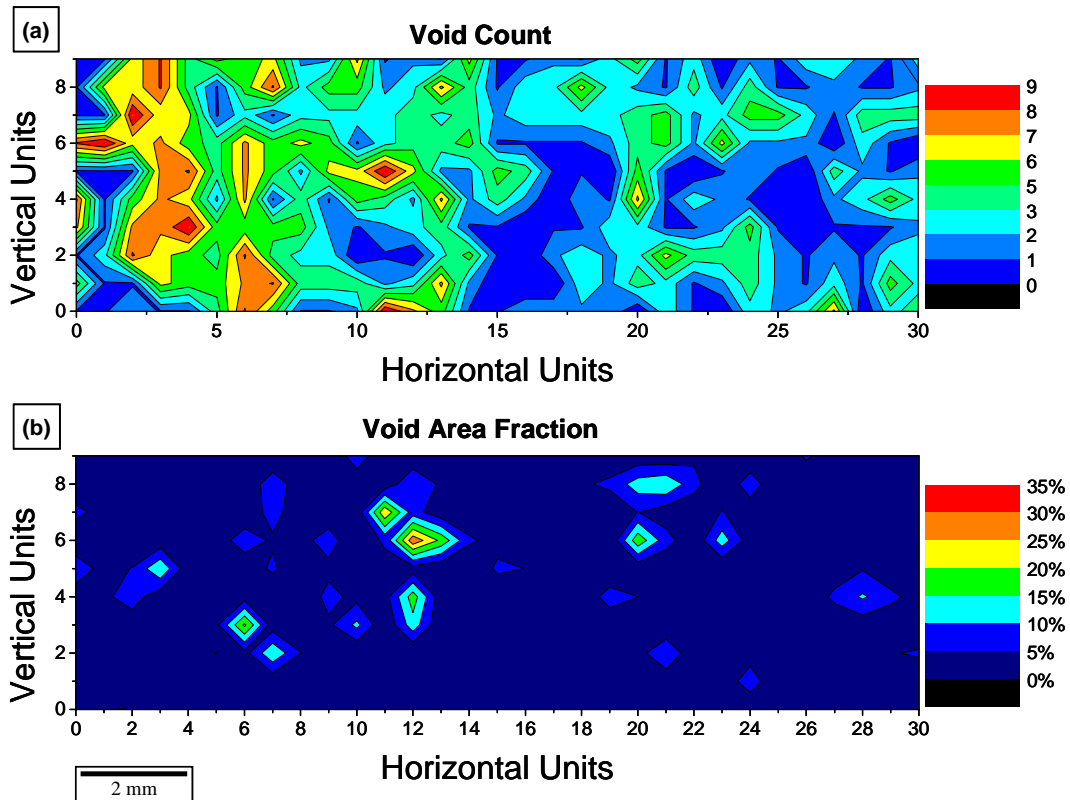


Figure 6 – Local mapping for axial sample. (a) Void count. (b) Void area fraction. Horizontal and vertical units refer to the count of 250x250 pixels windows in each direction. See text for details.

In this analysis, the neighborhood of each relevant object, a void in this case, is analyzed and its nearest neighbors are identified by the so-called tessellation technique [11]. See Figure 7 for the sequence steps shown in a small section of one of the mosaics. The original grayscale image (Figure 7a) is segmented and post-processed as described above, leading to a binary image showing the voids (Figure 7b). All particles are then simultaneously dilated until a one pixel boundary is left around each particle (Figure 7c). This technique is based on the well-known Voronoi diagram [12]. Through a sequence of dilation and intersection, the neighboring regions to any given reference region can be automatically identified. Another intersection operation shows the corresponding original voids (Figure 7d). Then, the edge to edge distances between the reference void and its nearest neighbors are obtained (Figure 7e). A set of vectors is obtained for each void (Figure 7f) and the sequence is repeated for each and every void.

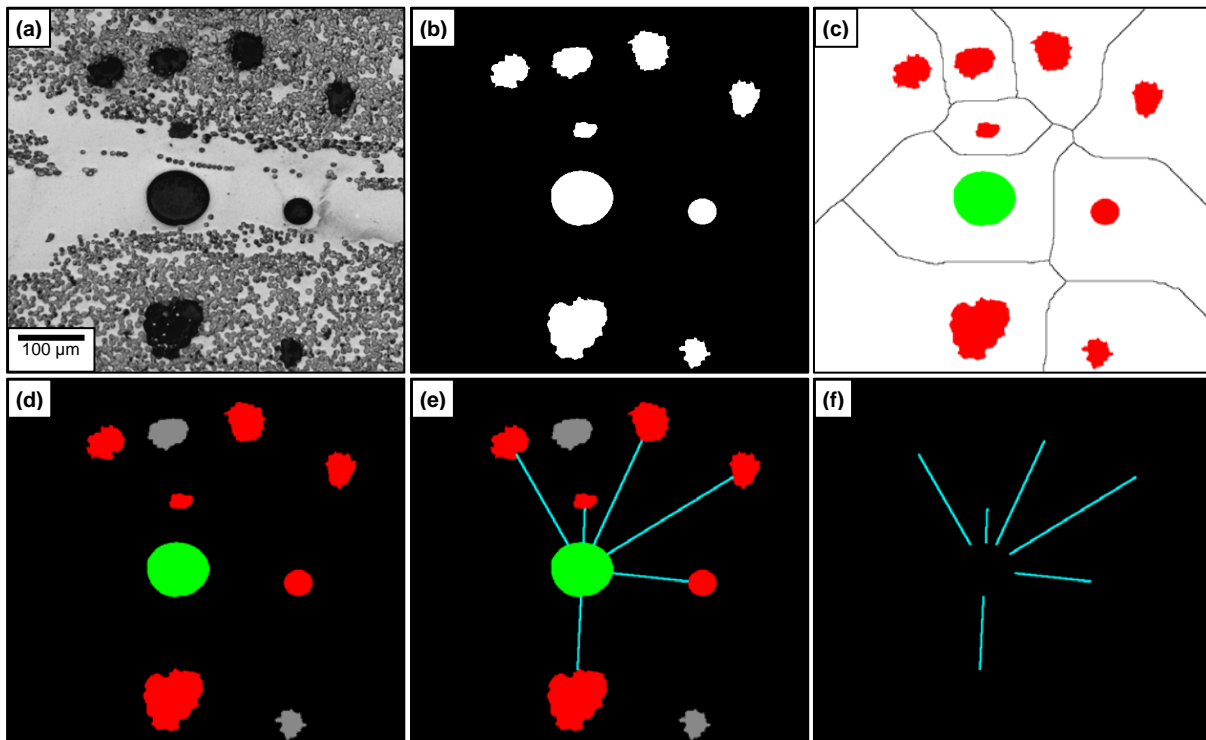


Figure 7 – Image processing sequence to measure void nearest neighbors' distances. (a) Original image fragment. (b) Detected voids. (c) Voids (in color) superimposed on their regions of influence. The reference void is shown in green. (d) Detection of nearest neighbors (shown in red). Grey voids are not nearest neighbors. (e) Determination of distances between reference void and its neighbors. (f) Distribution of distances.

Thus, a distribution of distances is measured for each void, with its average and standard deviation. The coefficient of variation (*cov*) is defined as the ratio of the standard deviation to the average distance. It has been shown previously [11] that for a uniform random spatial distribution  $cov = 0.36 \pm 0.02$ . Deviations from this value indicate some degree of clustering of the analyzed phase.

For the circumferential and axial samples shown, respectively, in Figures 2 and 3, the values obtained were  $cov = 0.37$  and  $cov = 0.50$ . These results confirm the qualitative analysis that indicated that the spatial distribution of voids was almost perfectly random for the circumferential sample while the axial sample showed substantial clustering.



### 3.2 Fiber and Layer Analysis

Figure 8a shows a typical mosaic obtained operating the SEM in BSE mode. The contrast between fibers and matrix is sharp and one can easily distinguish fibers in different orientations, and the several layers resulting from filament winding. This image has undergone background correction to eliminate intensity variations between the several image tiles and noise filtering. The details of the procedure are described elsewhere [13].

Fibers were automatically discriminated by their gray shade, as shown in Figure 8b. A few steps of post-processing were necessary to eliminate spurious objects in the background and holes in fibers. Boundaries between touching fibers were also obtained by the traditional watershed method [14].

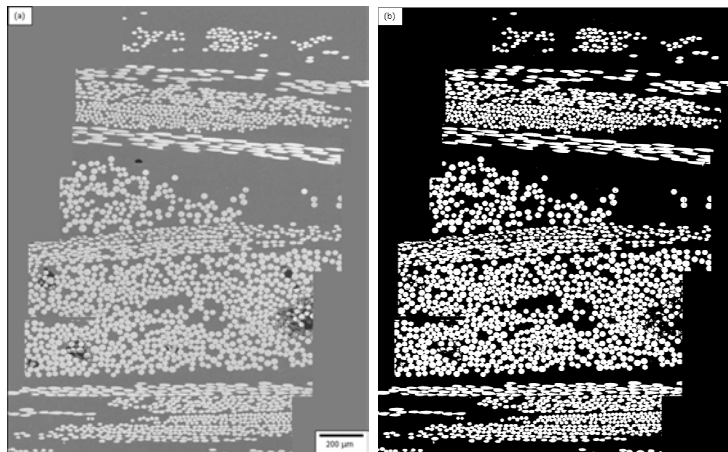


Figure 8 – (a) Example of a mosaic image obtained by assembling 28 (4x7) individual images, after equalizing the illumination of each field. (b) Fiber discrimination.

Once fibers were accurately detected, a sequence of image processing operations was employed to discriminate layers. The basic principle behind this discrimination was the separation by fiber shape. Fibers normal to the image plane appear round, while fibers inclined relative to this plane appear as ellipsoids. Thus, shape parameters such as the aspect ratio and the circular shape factor [8] were used. Thus, the original image was separated into two intermediate images containing normal and inclined fibers. See Figure 9.

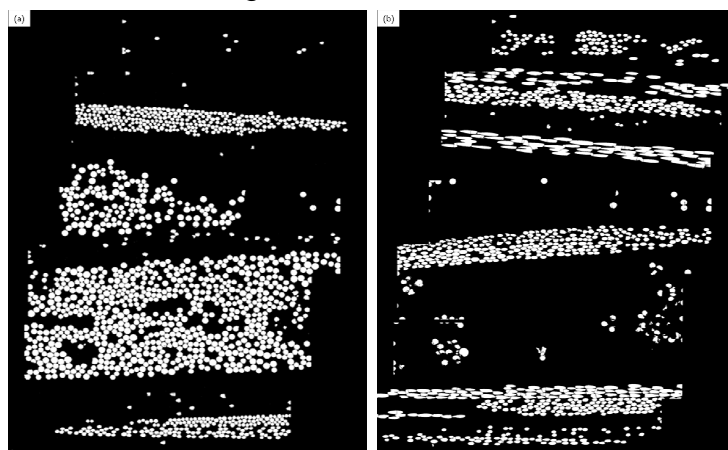


Figure 9 – (a) Fibers normal to the image plane. (b) Fibers inclined to the image plane.

A sequence of morphological operations was then applied to join neighboring fibers, eliminate stray or broken fibers, and detect each fiber layer. The details are described elsewhere [13]. The result is shown in Figure 10, where each layer is identified by a different color, superimposed on the original image.



The winding angle of each fiber can be obtained through the measurement of its major and minor projections ( $F_{max}$  and  $F_{min}$ ) and the equation

$$\phi_{Fiber} = \arcsen\left(\frac{F_{min}}{F_{max}}\right) \cdot \left(\frac{180}{\pi}\right)$$

The winding angle of a layer is estimated as the average of the winding angles of all fibers that belong to that layer. The results are show in Table 1, where one can see that a nonsymmetrical stacking sequence was used. From a mechanical behavior point of view this is not a good result, since nonsymmetrical laminates have bending-stretching coupling that can cause warping due to in-plane forces [15].

It is apparent from the results listed in Table 1 that larger standard deviations were found for the layers with more inclined angles (especially layers 3, 8, and 11). This is consistent with the comments above, regarding the difficulty to separate touching fibers in these layers. In certain cases, the separation lines of the watershed method break elongated fibers, creating objects with varying shapes within a layer, and thus biasing the winding angle measurement.

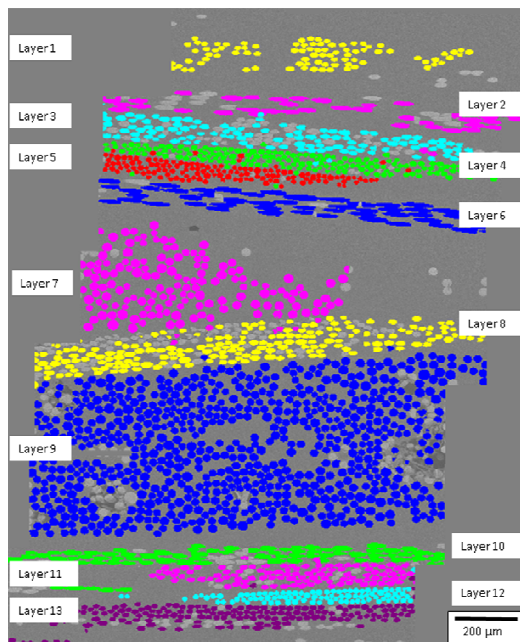


Figure 10 – Final discrimination of fiber layers according to fiber orientation.

Table I – Winding angles of the fiber layers

Layer #	Angle (degrees)*
1	38.8 ± 4.9
2	14.0 ± 3.8
3	34.4 ± 11.4
4	49.4 ± 5.0
5	63.6 ± 5.3
6	10.5 ± 3.2
7	63.0 ± 4.6
8	36.6 ± 10.5
9	63.2 ± 4.0
10	7.5 ± 4.0
11	36.9 ± 10.1
12	64.9 ± 2.8
13	41.2 ± 8.8

\*Angle is shown as average ± standard deviation

The methodology of identification of the actual lamina stacking sequence, however, proves its robustness, since the microstructural characterization of the entire cross section can be used to monitor deviations from the manufacturing designed lamina stacking sequence. A correction in the fabrication routine can thus be made, and better quality pipes can be manufactured.

#### 4. CONCLUSIONS

The use of mosaic images covering the entire cross section of the fiber-reinforced composite was fundamental to reveal the complete microstructural arrangement, showing the spatial distribution of voids and fibers.

The developed methodology was able to discriminate voids from preparation defects, and obtain their spatial distribution in a quantitative way. It was also possible to identify each individual lamina wound during the manufacturing process of a composite pipe. The image processing and analysis procedure developed to

measure fiber size and shape allowed the determination of the average winding angle for each identified layer.

## ACKNOWLEDGMENTS

The support of CNPq is gratefully acknowledged.

## REFERENCES

1. Hamidi, Y.K. and Altan, M.C. (2003). Spatial variation of void morphology in resin transfer molded E-glass/epoxy composites, *J. Mater. Sci. Letters* **22**: 1813-1816.
2. Santulli, C., Gil, R.G., Long, A.C. and Clifford, M.J. (2002). Void content measurements in commingled E-glass/polypropylene composites using image analysis from optical micrographs, *Sci. Eng. Comp. Mater.* **10**: 77-90.
3. Saint-Martin, G., Schmidt, F., Devos, P. and Levailant, C. (2003). Voids in short fibre-reinforced injection-moulded parts: density control vs. mass control. *Polym. Testing* **22**: 947–953.
4. Bai, J., Hu, G. and Bompard, P. (1997). Mechanical behaviour of  $\pm 55^\circ$  filament-wound glass-fibre/epoxy-resin tubes. *Comp. Sci. Technol.* **57**: 155-164.
5. Cilley, E., Roylance, D. and Schneider, N. (1974). Methods of fiber and void measurement in graphite/epoxy composites. In *Composite Materials: Testing and Design (Third Conference)*, ASTM STP 546, American Society for Testing and Materials, 237-249.
6. Purslow, D. (1984). On the optical assessment of the void content in composite materials. *Composites* **15**: 207-210.
7. McCarvill, W.T. (1987). Filament-winding resins. In *Engineered Materials Handbook – vol.1 Composites*, ASM International, Metals Park, 135-138.
8. Paciornik, S. and Mauricio, M.H.P. Digital Imaging. (2004) In *ASM Handbook: Metallography and Microstructures*. ASM International, Materials Park, 368-402.
9. Vander Voort, G. F. (2000). *Metallography, Principles and Practice*. ASM International, Materials Park.
10. Paciornik, S. and d'Almeida, J.R.M. (2009). Measurement of void content and distribution in composite materials through digital microscopy. *Journal of Composite Materials*, **43**(2): 101-112.
11. Yang, N., Boselli, J. and Sinclair, I. (2000). Simulation and quantitative assessment of homogeneous and inhomogeneous particle distributions in particulate metal matrix composites, *J. Microsc.* **201**: 189-200.
12. Shehata, M. T. (2000). Characterization of Particle Dispersion. In *Practical Guide to Image Analysis*. ASM International, Materials Park, 129-144.
13. De Oliveira, J.G.A. ; Paciornik, S. ; D'Almeida, J.R.M. (2009). Microstructural Analysis of Composite Tubes through Digital Microscopy. *Journal of Composite Materials*, **43**,1857-1868.
14. Beucher, S. and Lantéjoul, C. (1979). Use of watersheds in contour detection. Proceedings of the International Workshop on Image Processing, Real-time Edge and Motion Detection/Estimation, 2.1-2.12, Rennes, France.
15. Gibson, R.F. (1994) *Principles of Composite Material Mechanics*. McGraw-Hill, New York, NY.